Evolution of Morphology and Grain Structure of Metal Nanowires in Initial Period of Templated Electrodeposition

A. Leontiev, D. Bograchev, D. Khmelenin, G. Tsirlina, K. Napolskii

Evolution of Morphology and Grain Structure of Metal Nanowires in Initial Period of Templated Electrodeposition

A.P. Leontiev,[a,b,c] D.A. Bograchev,[a] D.N. Khmelenin,[d] G.A. Tsirlina,[b,e] K.S. Napolskii[b,c,*]

[a]Department of Chemical Sciences, Faculty of Natural Sciences, Ariel University, 40700, Ariel, Israel

[b]Department of Chemistry, Lomonosov Moscow State University, 119991 Moscow, Russia

[c]Department of Materials Science, Lomonosov Moscow State University, 119991 Moscow, Russia

[d]Shubnikov Institute of Crystallography of Federal Scientific Research Center 'Crystallography and Photonics', Russian Academy of Sciences, 119333, Moscow, Russia

[e]University Grenoble Alpes, University Savoie Mont Blanc, CNRS, Grenoble INP, LEPMI, 38610, Grenoble, France

*Corresponding Author: kirill@inorg.chem.msu.ru

Abstract

Templated electrodeposition is one of the most effective ways to prepare arrays of one-dimensional nanostructures. The growth of the nanostructures can be monitored *in situ* in the course of electrodeposition by analysing the current-time transients. However, the analysis of nonmonotonic current behaviour corresponding to nucleation and initial growth of the nanostructures is rarely discussed in the literature. Here, the detailed study of the initial stages of templated electrodeposition of Au inside the pores of anodic aluminium oxide is performed. The experimental tools to visualize the nanostructures formed in initial period are proposed based on the scanning and transmission electron microscopy data. The observed features of deposition transients are associated with the changes in both the morphology and grain structure of the deposit and are also affected by parallel hydrogen evolution. The experimental observations are supported by the numerical simulations.

1. Introduction

One of the possible ways to prepare arrays of one-dimensional metallic nanostructures (e.g., nanorods, nanowires, and nanotubes) is templated electrodeposition [1], which combines the advantages of template synthesis and electrodeposition technique. The diameter and spatial

distribution of the nanostructures are determined by the structure of porous template, the length of metal nanostructures depends on the charge passed during electrodeposition, and the microstructure of the metal is controlled by the deposition potential [2, 3]. Porous anodic aluminium oxide (AAO) is a conventional template for the formation of arrays of anisotropic nanostructures, being advantageous due to the ordered arrangement of pores with a narrow size distribution [4], as well as to its high thermal, mechanical, and chemical stability [5, 6].

In order to use dielectric AAO films as templates for controlled DC electrodeposition (here we discuss electrodeposition under DC mode exclusively), one side of the AAO should be covered with electron-conductive material, which acts as a current collector. The nucleation and growth of a new phase during electrode polarization is accompanied by the appearance of a non-stationary diffusion flow of electroactive species (e.g., metal ions) and by corresponding current decrease. In the limiting current regime, the current-time transient is well described by the Cottrell equation [7-11]. The diffusion front rapidly approaches the external surface of the template and moves into the bulk of the electrolyte solution. Since the pores in the AAO are closely packed, the diffusion zones of individual pores overlap, forming a united outer diffusion layer [12]. The AAO pore diameter is usually smaller than 200 nm, which allows one to neglect convective mass transfer inside the pores due to viscosity effects. However, forced or natural convection outside the template limits the thickness of the outer diffusion layer [13]. Therefore, one can assume that linear concentration profiles are established in the pores and in the outer diffusion layer outside the template, and electrodeposition proceeds under a quasi-stationary mode.

The growth of metal in AAO leads to a decrease in the length of still unfilled part of the pores and, as a consequence, to a thinning of the diffusion layer. Therefore, slow current increase is observed in the overall time interval [11, 14, 15], excluding a short initial period discussed below. At a certain moment some pores appear to be completely filled, and metal starts to grow on the external surface of the template, inducing a sharp current increase. Simultaneously, the shorter nanowires that were not in time to reach the top surface of the template, stop growing due to the screening effect [11]. As a result, typically the total degree of AAO pore filling is significantly lower than 100%.

The analysis of current transients and, in particular, their initial parts responsible for the nanostructures nucleation and early stages of the growth near bottom of the pores, is rarely discussed in the literature. One of less understood features is the current maximum usually observed in several seconds after the start of templated electrodeposition. For a number of systems [16, 17], this maximum was associated with nucleation and analysed within the Scharifker-Hills model [18], which describes three-dimensional diffusion-controlled nucleation on bare electrodes. However, this approach is

questionable because the geometry of templated electrodeposition differs significantly from that of a planar electrode. The diffusion zones of nuclei located in the same pore start to be limited by the pore walls at times of the order of 1 μs. Based on these considerations, the initial current increase cannot be explained in terms of instantaneous diffusion-controlled nucleation. At the same time, current increase is basically possible in case of progressive "activation" of the pores, i.e. if the electrodeposition process in various pores does not start simultaneously. In addition, models of nucleation under kinetic mode [19] can be applied. In this case the effect of template is reduced to the change of the available electrode area.

The appearance of the current maximum can be also associated with the specific geometry of the growing deposit at the early stages, e.g. when metal grows in the form of nanotubes [20-23]. Actually, the initial current increase can follow the increase in the surface area of a newly formed metallic tube. Then the convergence and coalescence of the walls of the nanotube result in the decrease of current and appearance of the maximum. The subsequent region of the steady-state current starts when the nanotubes transform into nanowires with smaller intrinsic surface area at their edges, which remains unchanged when wire length continues to increase. It is worth noting that if a discontinuous metal layer is used as a current collector, the maximum in the current transient is associated with the transition from metal growth "under the template" to the formation of nanowires [23].

We report the detailed study of the initial stages of Au templated electrodeposition inside the pores of AAO templates. Experimental tools to visualize the bottom part of the deposited nanostructures are proposed based on the scanning and transmission electron microscopy. We demonstrate that metal deposition in the system under study starts from the formation of nanotubes due to location of the sputtered current collector material on the bottom parts of the pore walls. The observed features of deposition transients are associated with the changes in both the morphology and grain structure of the deposit and also affected by parallel hydrogen evolution. The experimental observations agree qualitatively with the numerical simulations predicting the transition of the morphology of growing nanostructures from nanotubes to nanowires.

2. Experimental part

Porous AAO films were prepared by two-step anodizing of high-purity (99.99%) electropolished aluminium foils in 0.3 M $H_2C_2O_4$ electrolyte at a voltage of 40 V and the electrolyte temperature of 0 °C as described elsewhere [13]. The thickness of a sacrificial AAO layer formed during the first anodizing step was 20 μm. After the second anodizing process the residual aluminium was selectively dissolved in a mixture of CH_3OH and Br_2 with a volume-to-volume ratio of 10 : 1.

Then the barrier AAO layer was etched away in 0.3 M H_3PO_4 using the electrochemical detection of pore opening [24]. Once the pores were opened, additional etching was carried out to control the porosity (*p*) of AAO templates. AAO films of the thickness of 35 and 50 μm with *p* of 40 and 20%, respectively, were used in the electrochemical experiments.

At the next step, Au current collector was formed on the bottom surface of the AAO templates using Leybold z400 (Polifab) magnetron sputtering system. To improve gold adhesion, two-step deposition process was applied. Initially, the chamber was pumped down to $2 \cdot 10^{-6}$ mbar and then filled with Ar up to the pressure of $1.2 \cdot 10^{-2}$ mbar. After the cleaning of the AAO films in Ar^+ plasma, a sacrificial 30-nm-thick Au layer was sputtered in the same vacuum cycle. Then the sacrificial layer was etched away by Ar^+ plasma. During the second sputtering step, a continuous Au layer was formed. The major part of the sputtered material (average thickness of 240 nm) is deposited onto the outer surface of the AAO template, but there are no doubts that penetration of gold into the pores is unavoidable [25].

Gold was electrodeposited in a three-electrode cell from a commercial electrolyte (purchased from Ecomet, Russia) containing 0.05 M $[Au(CN)_2]^-$ in citric buffer solution (pH = 6). The electrolyte was continuously agitated by a magnetic stirrer. Pt wire ring parallel to the cell bottom, and a saturated Ag/AgCl electrode were used as a counter and reference electrodes, respectively. The deposition was carried out at a constant deposition potential of −1 V (here and below the electrode potentials are reported vs. saturated Ag/AgCl electrode). The reported currents are normalized to the geometric surface area of the electrode, 0.25 cm^2, independently of AAO porosity. The electrochemical measurements were carried out using Autolab PGSTAT100N (Metrohm) potentiostat. The current efficiency of the electrodeposition was estimated gravimetrically using GR-202 (AND) analytical balance with 0.1 mg accuracy.

The morphology of the Au/AAO nanocomposites was studied using a scanning electron microscope (SEM) Supra 50 VP (LEO). Prior to SEM investigations 5-nm-thick Cr layer was deposited on the surface of the samples by magnetron sputtering. To visualise the bottom surface of the nanocomposites, the external part of the current collector was etched away in Ar^+ plasma.

Transmission electron microscopy (TEM) was carried out using a Tecnai Osiris microscope (FEI). The cross-section lamella of specimens for TEM was fabricated by focused ion beam (FIB) using a dual beam Helios Nano Lab 600i microscope (FEI). Pt layer was sputtered onto the sample surface to prevent its etching during the process of the lamella preparation.

3. Simulation

The discharge of $[Au(CN)_2]^-$ at low overpotentials can be complicated by the formation of adsorbed intermediates [26-29]. Formal potential of −0.605 V was reported for $[Au(CN)_2]^-$/Au [27], equilibrium potential can be estimated as −0.72 V. This means that we are dealing with deposition at rather high overpotentials of 0.28 – 0.4 V, therefore, more simple reaction pathway can be considered. The developed model of templated deposition assumes electron transfer and the preceding diffusion steps, not complicated by migration and adsorption steps. It is assumed that the deposition under mixed mode occurs at the metal/electrolyte interface following the Tafel law, and the current density can be presented in terms of the kinetic length [14]:

$$i = -i_0 \frac{c^s}{c^*} \exp\left(-\frac{\alpha F \eta}{RT}\right) = -F \frac{c^s}{\delta_k} D, \quad (1)$$

where $\delta_k = \frac{F c^* D}{i_0} \exp\left(\frac{\alpha F \eta}{RT}\right)$ is the kinetic length, c^* is the bulk concentration of the gold reagent, c^s is its interfacial concentration, D is the diffusion coefficient, i_0 is the exchange current density. The kinetic length (which plays a role of additional diffusion length) is a value of the distance dimension, which depends on the kinetic parameters and reflects the contribution of electron transfer step [30]. If δ_k tends to zero, the reaction occurs under diffusion mode. This kinetic length is convenient for the analysis of deposition in nanopores as, in fact, it is an effective diffusion length when summed with the thickness of the template and of the outer diffusion layer [11, 12, 14, 31].

Thus, the boundary conditions at the gold surface were assumed to be the electrodeposition reaction associated with the Tafel kinetics (Eq. 1) and the bulk reagent concentration at the mouth of the pore c^*. The outer diffusion layer is usually thicker than the template itself and significantly affects ions transport in the nanopore [12, 13]. To consider the presence of the outer diffusion layer, the length of the pore was assumed to be 120 μm.

The initial concentration distribution in the pore was assumed to be the same as in the bulk. The initial electrodeposition region was taken as the bottom of the pore and a specific cylindrical region with a height H. On the nanopore walls free from sputtered metal, no deposition was supposed due to insulating walls surface. Single pore was simulated assuming that all pores are identical, and the growth of the Au phase starts simultaneously in all pores. These simplifications are necessary at this stage to identify the role of gold at the walls in frames of more transparent model.

Changes in the gold/electrolyte boundary are taken into account using the level-set method [32, 33]. The calculations were carried out in the COMSOL Multiphysics package using cylindrical

coordinates to simulate two-dimensional diffusion fluxes. The parameters used for the simulations are summarized in Table 1.

Table 1. Parameters used for the simulations.

Parameter	Value
Diffusion coefficient, D, [$cm^2 \cdot s^{-1}$]	10^{-5}
Bulk concentration, c^*, [$mol \cdot l^{-1}$]	0.05
Kinetic length, δ_k, [μm]	0.1 – 15
Pore diameter, d_p, [nm]	50
Initial height of the deposition cylindrical region, H, [nm]	$d_p - 4d_p$
Effective length of model, [μm]	H + 120
Metal density, [$kg \cdot m^{-3}$]	19300
Metal molar mass, [$kg \cdot mol^{-1}$]	0.197

4. Results and discussion

For preliminary characterization of the kinetics of gold templated electrodeposition, cyclic voltammograms were recorded at various solution stirring rates (Fig. 1). At potentials more positive than −0.9 V, the current density shows minimal sensitivity to external stirring, suggesting mostly kinetic control of electrodeposition. At more negative potentials, current density increases rapidly with overpotential and pronounced dependence on the stirring rate is observed. Within the range of E < −1.3 V current density increase slows down. This behaviour is likely due to the partial blocking of pores and/or the external surface of the template by hydrogen bubbles generated by side reaction of H_3O^+ reduction.

It is worth noting that a current shoulder is observed in the voltammogram at the potential of −1.15 V. It looks less pronounced due to the background current of hydrogen generation. This side reaction considerably reduces the current efficiency of gold electrodeposition. For instance, already at the potential of −1 V, the current efficiency is (49.3 ± 0.5)%. In the vicinity of the shoulder the current density depends on the rate of solution stirring, suggesting a possible transition of gold electrodeposition to the diffusion regime. To estimate the limiting diffusion current density of gold electrodeposition, the following equation can be used [34, 35]:

$$-\frac{1}{i_{d,lim}} = \frac{\phi}{pnFDc^*} + \frac{\delta}{nFDc^*}, \quad (2)$$

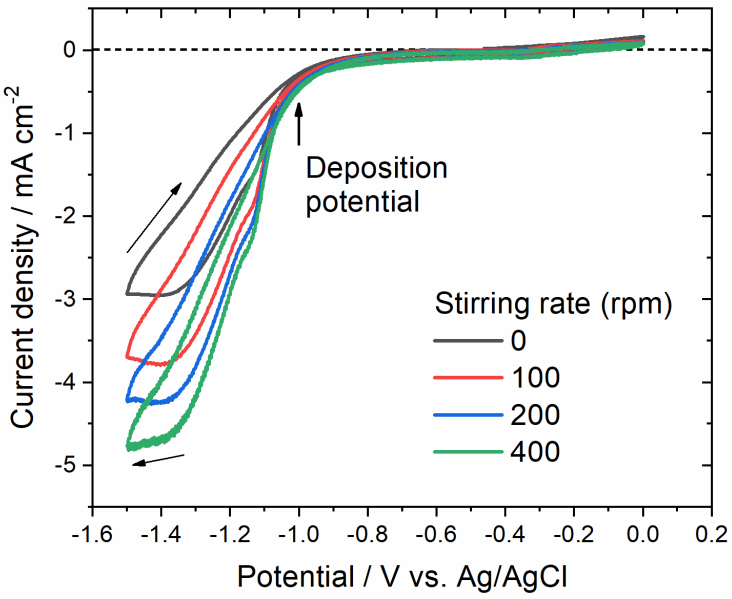

Figure 1. Cyclic voltammograms (CVA) for Au electrode covered with 50 μm-thick AAO template (p = 20%) recorded in 0.05 M $[Au(CN)_2]^-$ solution in citric buffer (pH = 6) at the scan rate of 20 mV/s and various stirring rates of electrolyte. The third cycle for each CVA curve is presented.

where ϕ and p are the thickness and porosity of the template (50 μm and 20%, respectively), F is the Faraday constant (96485 C/mol), δ is the thickness of the outer diffusion layer (estimated as 200 μm based on the diffusion current of copper templated electrodeposition in the pores of an identical template conducted in the same cell at a stirring rate of 400 rpm). Assuming the diffusion coefficient to be $1.67 \cdot 10^{-5}$ $cm^2 \cdot s^{-1}$ [26], according to the Equation 2, limiting diffusion current density for AAO sample presented in Fig.1 equals to −1.8 mA/cm^2 (per geometric area), which aligns with the observed current density at the potential of −1.15 V, considering the current efficiency. Hence, it can be concluded that the shoulder manifests the limiting diffusion current.

The potential of −1 V was selected to achieve a relatively high rate of metal growth while maintaining a moderate rate of hydrogen generation. According to the literature, at this relatively high overpotential, gold electrodeposition predominantly occurs via the direct transfer of electron to the $[Au(CN)_2]^-$ anion [26, 28]. Figure 2 presents the current-time transients of two consecutive templated gold electrodepositions into the same AAO template. After a rapid decrease in current during the initial few seconds period of the first deposition, one can see a current growth followed by a maximum at ca. 20 s. Subsequently, the current density gradually decreases and reaches a steady state only after ~200 s from the start of the first electrodeposition (red curve in Fig. 2). The second electrodeposition was carried out into the same template after five minutes delay under open circuit conditions. In this

case, no specific transient features were observed (blue curve in Fig. 2): the current demonstrated a stationary value, the same as observed at the end of the first deposition.

The initial current decrease can be attributed to a decrease in the interfacial reagent concentration, whereas the nature of the maximum is less evident. Formally, it looks similar to the nucleation maximum typical for metals deposition on the plane electrode [36]. According to the Cottrell equation, diffusion zones in a single pore with a diameter of 70 nm should overlap in ca. 1 μs, whereas the characteristic time of the overlapping of diffusion zones of neighbouring 35 μm-long pores is six orders longer, i.e. approximately 1 s. Thus, the Scharifker-Hills model of nucleation cannot explain the current maximum in Fig. 2 (more roughly, it cannot be applied in case of 1D diffusion, which dominates in the pores at not too low time). One cannot exclude that kinetically-controlled nucleation models [36] may work. Actually, for steady-state nanowires growth rate to be ca. 2 nm/s (as estimated from the current in Fig. 2), single 3D nucleus approaches the pore walls in ca. 17.5 s. However, the observed dependence on solution convection does not allow to consider purely kinetic

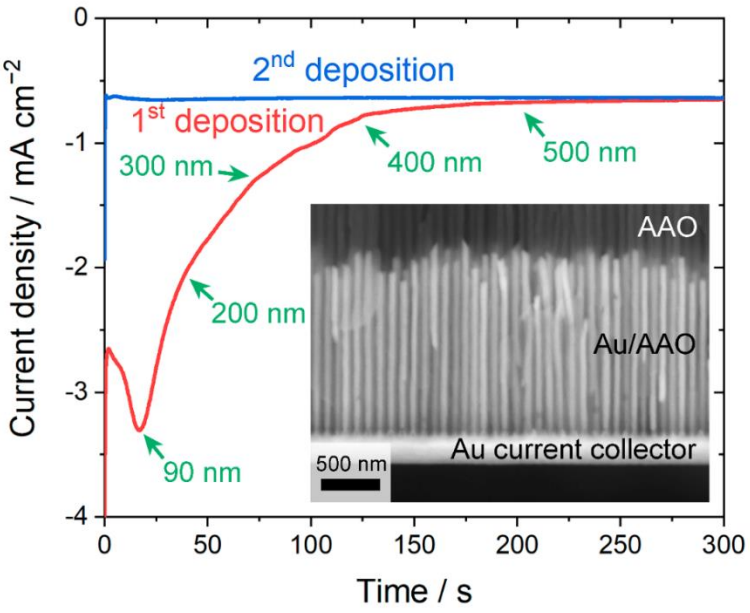

Figure 2. Current-time transients registered during two successive gold electrodepositions in the pores of one and the same 35 μm-thick AAO template (p = 40%). The electrodepositions were carried out under intensive stirring at the potential of −1 V vs saturated Ag/AgCl reference electrode from 0.05 M $[Au(CN)]^{2-}$ in citric buffer solution (pH = 6). Second deposition was started after five minutes-long pause under open circuit. Estimated length of the nanowires at various times is indicated. The inset is a cross-sectional SEM image of the resulting Au/AAO nanocomposite.

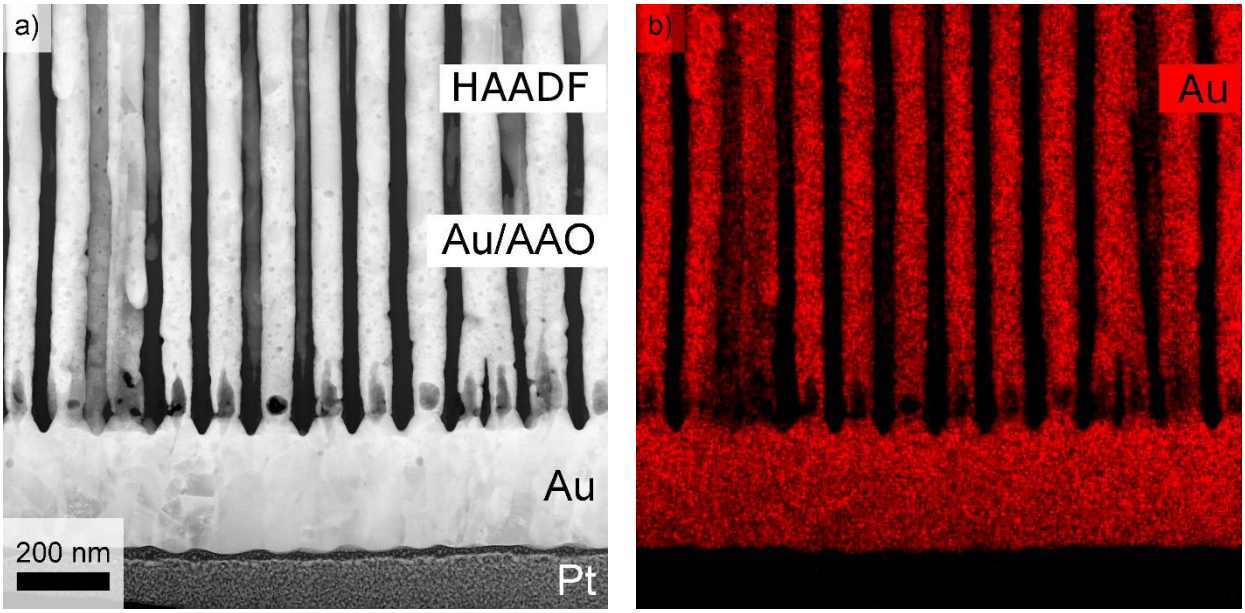

Figure 3. TEM image of a cross-section lamella of Au/AAO nanocomposite (a) and corresponding energy dispersive X-ray spectroscopy map of Au distribution (b).

mode. In what follows we consider various possible reasons of nonmonotonic current transients observed for Au templated electrodeposition with account for morphological features.

To start this analysis, the bottom part of the nanowires was imaged. TEM image of a cross-section lamella prepared using focused ion beam is presented in Figure 3. The voids in the bottom part of nanowires are clearly seen. The estimated deposition charge, with account for current efficiency, demonstrates that the voids are formed just in the region corresponding to the maximum at current transient. Thus, the following preliminary hypothesis can be formulated. The metal starts to grow in the form of nanotubes, resulting from the partial sputtering of the material of current collector onto the pore walls: nucleation and growth at these sputtered fragments results in preferential metal deposition along the pore walls, inducing the increase in gold surface area and deposition current. Under diffusion or mixed mode, the upper parts of the nanotube walls thicken faster due to the better accessibility for $[Au(CN)_2]^-$ reagent as compared to bottom part of the pores. Correspondingly, tube internal diameter narrows in its upper part, even stronger aggravating accessibility difference and decreasing the surface available for deposition, so the current starts to decrease. At a certain point the walls of the nanotubes merge, and the deposit real surface area reaches a steady value close to the area of the pore cross-section. The subsequent (second) deposition starts at already established surface, and the changes of current appear to be minimal (see blue curve in Fig. 2).

Alternatively, the current maximum could also be explained by considering the progressive activation of the pores. Within this assumption, the surface area grows due to an increase in the density

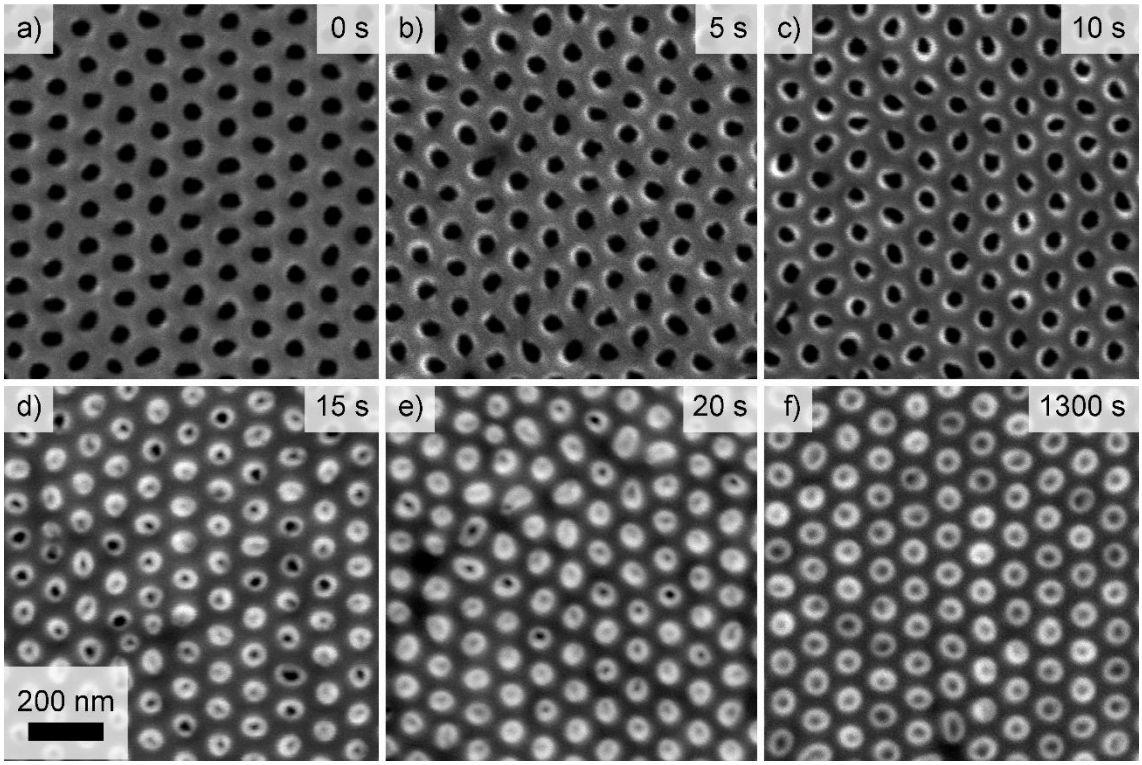

Figure 4. The morphology of the bottom surface of Au/AAO nanocomposites formed at different deposition durations. The current collector was selectively etched away in Ar^+ plasma prior to SEM studies.

of "active" pores, while, conversely, it diminishes due to a gradual transition from nanotubes to nanowires. A specific combination of these opposing processes parameters could potentially lead to the occurrence of the current maximum.

To trace accumulation of gold in the bottom part of nanostructures, a series of samples was fabricated with various electrodeposition durations to analyse the evolution of gold morphology. The SEM images of the bottom surface of the samples after the removal of the current collector in Ar^+ plasma are presented in Figure 4. It is well-seen that gold initially grows in the form of nanotubes. The thickness of the nanotube walls slightly differs for various pores of each sample (each deposition time). However, all the pores seen in one image (about a hundred) are active, and for almost all the pores the continuous nanotube walls form after 10 s. One can assume that the number of inactive pores (if any) does not exceed 1%, so the effect of pores 'activation' can hardly play an essential role. The thicknesses of the nanotube walls after 20 s (which is close to the time of current maximum in Fig. 2) and after much longer deposition (1300 s) are similar, which means that after 20 s metal growth does not affect the walls of nanotubes.

The length of the nanowires corresponding to current maximum, as estimated from the deposition charge and total length of the nanowires (see inset in Fig. 2), is ca. twice the diameter of

the pores (Fig. 2), which agrees well with TEM observations (Fig. 3). Therefore, it can be assumed that almost all the nanowires are already formed by the 20th second, and the transport of metal-containing ions to the nanotube bottoms is not possible any more. Thus, the real surface area of the deposited metal should be close to a steady state value.

Taking into account SEM observations, one can make the following conclusions:

i) the current increase is not related to progressive activation of pores; simultaneous activation of the pores occurs at least within a time scale of few seconds (Figure 4b);

ii) the current decrease cannot be attributed to the graduate transition from the nanotubes to nanorods (Figure 4e).

At the same time, the hypothesis attributing the current maximum to the change in the metal surface area and redistribution of diffusion fluxes agrees well with microscopy data and coulometric estimates. To verify this hypothesis independently, we report below the results of simulations for the metal growth under various mixed modes and for various height of the sputtered metal inside the pores. We do not pretend to complete quantitative agreement with experiment, as the real morphology of gold sputtered inside the pore remains unknown, and just this morphology plays a crucial role in the kinetics of tube formation. The goal of simulations is to understand the conditions required to make diffusion limitations near the pore bottoms responsible for transition from nanotube to nanowire growth, and to compare with our experimental conditions.

For numerical simulation of the morphology changes in the course of templated electrodeposition the COMSOL Multiphysics package was used. Simulations demonstrate that if the height of the current collector layer on the pore walls equals to the pore diameter, the formation of the nanotubes is possible strictly in the diffusion limiting regime of electrodeposition (Fig. 5a). The voids will not appear if the currents are lower than 99% of diffusion limit (Fig. 5b). A morphology of the bottom part of the nanostructures being close to the experimental observations can be expected if the sputtering depth is higher than several pore diameters (Fig. 5c). Although it is feasible considering the magnetron sputtering method, even for sputtering depth of $4d_p$, the current should be more than 90% of the limiting diffusion current (Figs. 5c,d). With account for the current efficiency of 49.3%, the experimentally observed steady-state current equals to only 12% of the limiting diffusion current (−2.8 mA/cm^2, as calculated using Eq. 2 for 35 μm thick AAO sample with 40% porosity). Basically, current value could be significantly higher at initial stage due to large real surface area resulting in higher kinetic contribution.

Model simulations demonstrate a principal possibility of voids formation in the course of electrodeposition for the system with a large aspect ratio of the conducting section sputtered during

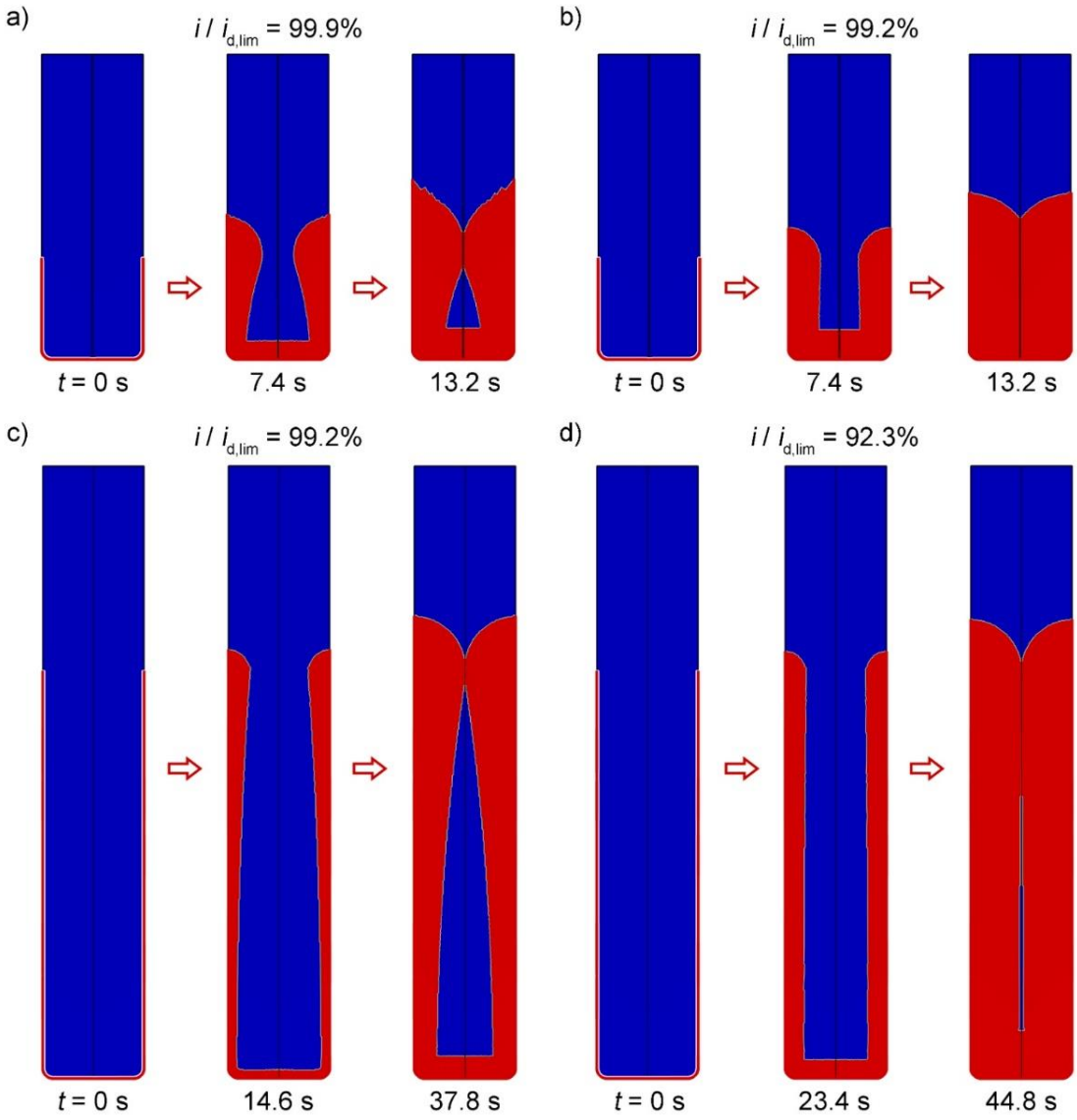

Figure 5. Numerical simulation of the metal morphology evolution during initial period of templated electrodeposition for the sputtering depth is equal to one (a,b) and four (c,d) pore diameters. The ratios of deposition current to the limiting diffusion current are given for each panel. Pore volume is blue, Au metal is red (for t = 0, a thin red layer is sputtered gold).

current collector fabrication or under conditions very close to the limiting diffusion current. Both required conditions do not agree quantitatively with experimental conditions of the observed voids formation. Moreover, there is an important qualitative contradiction of model prediction and experimental results.

Actually, in frames of applied model, the simulated current-time transients (Fig.6a) are monotonic, demonstrating Cottrell-like current decrease due to the relatively small height of the electroactive part of the pore compared to the effective diffusion length. At least in numerical simulations operating with idealized shape of the sputtered gold inside the pores, metal growth results

only in the decrease in the surface area due to the thickening of the nanotube walls (Fig. 6b). This does not allow to explain the appearance of current maximum in Fig. 2 (red curve) even if one assumes that the considerable variation of the current may be governed not by gold electrodeposition process, but by the side reaction of hydrogen generation (kinetically limited). Hence, we cannot abandon the assumption of the increase of the real surface area. This increase can be independently associated with the growth of electrodeposited metal on dispersed sputtered gold. According to microscopic data reported in Ref. [25], grain growth of gold inside the pores takes place, and the grains are reducing in size when located deeper from the template bottom surface. The depth of gold penetration in Ref. [25] was estimated as 1 μm. Surely some details of grains distribution depend on the sputtering geometry and mode, as well as on pore diameter. Qualitatively it is expected to be the same in our case: the amount of sputtered grains is higher near pore bottom, whereas at the upper part of the pore wall small grains are more rare and (starting from certain heights) mutually isolated. Assuming this configuration, electrodeposition can start only at coalesced sputtered grains located near the bottom. In the course of initial growth, electrodeposited metal reaches individual separated gold nanoparticles at the upper part of the wall, and the real surface available for further nucleation and growth appears. Similar starting configuration was reported for AAO templates with cell walls decorated by metal nanoparticles and used earlier for the controlled electrodeposition of long nanotubes [37].

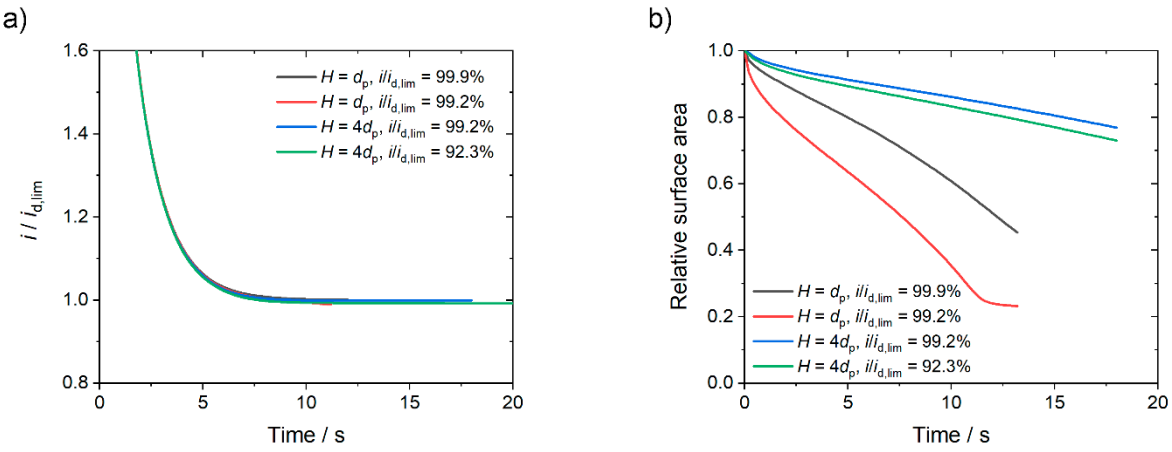

Figure 6. Numerical simulation of the current transients (a) and change in the surface area (b) during initial stage of electrodeposition. For (a) the current is normalized to the steady-state limiting diffusion current, for (b) the surface area is normalized to the surface area initially available for electrodeposition.

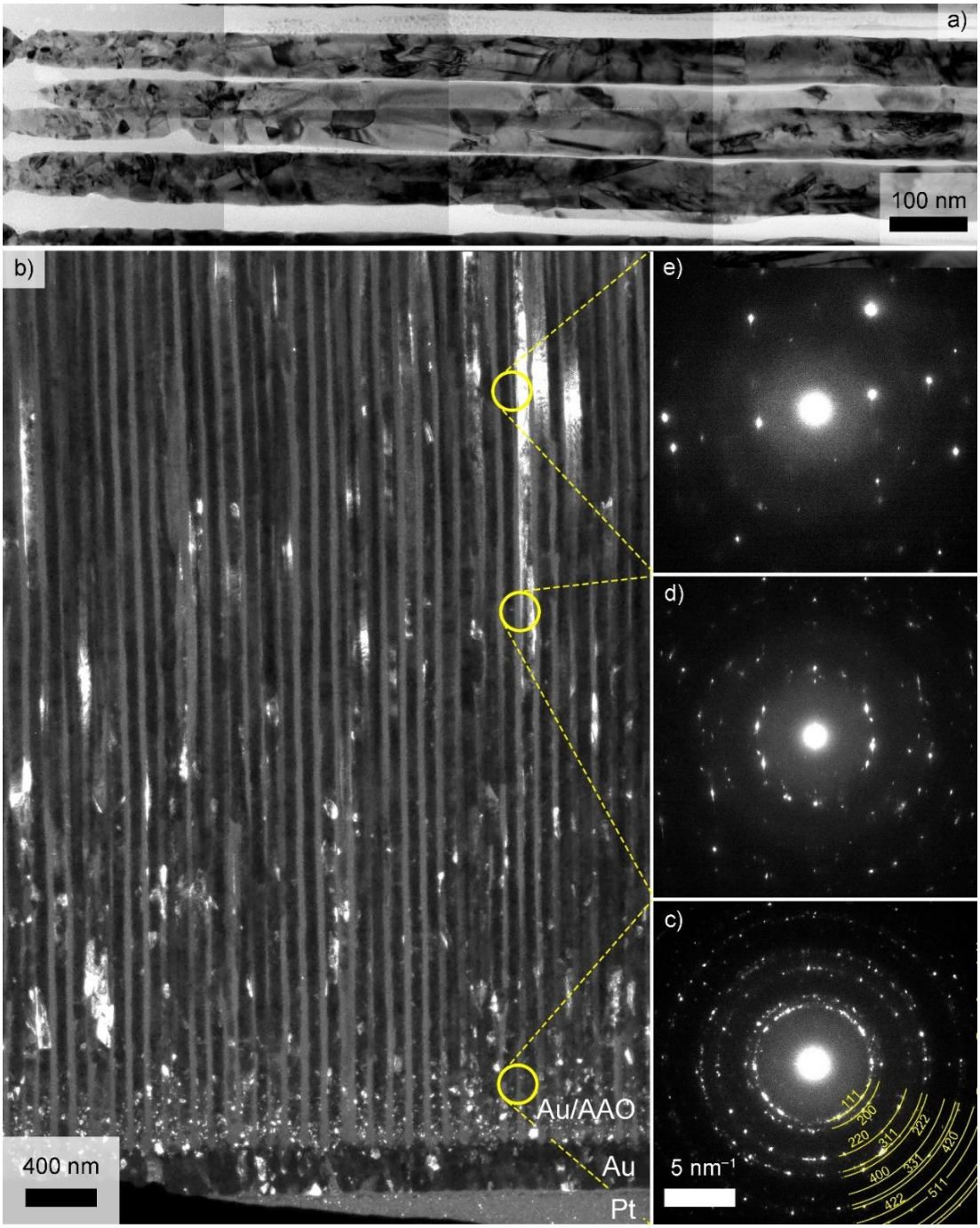

Figure 7. Bright- (a) and dark-field (b) TEM images of Au nanowires grown in AAO template and SAED patterns (c-e) recorded from different areas (indicated by yellow circles) along the nanowire growth direction.

Our assumption is confirmed by the fact that not only the morphology, but also the microstructure of the wires undergoes evolution in the course of templated electrodeposition. This follows from high-resolution and dark-field TEM images of the base part of Au nanowires (Fig. 7 a, b). This evolution can be understood taking into account that magnetron sputtered material forms small misoriented particles at the pore walls, assuming oriented growth of low-index crystallographic

grains typical for the system under study [29]. As a consequence, several nuclei can form in each pore, leading to the "faceting" of the pores (Fig. 4, deposition time 10 s). Then Au particles grow up and coalesce with each other, forming the walls of nanotubes and, further, the bottom part of the nanowires. Thus, in the initial stage, the electrodeposited metal inherits the polycrystalline structure of the current collector.

Experimental prove of the evolution of Au grain structure along the wire was not only observed by TEM, but also confirmed by the selected area electron diffraction (SAED) patterns. An almost "powder" diffraction pattern registered near the bottom of the nanowires (Fig. 7c) gradually transforms to a pattern characteristic for a "coarse-grained" structure (Fig. 7d, e). According to the darkfield image, the length of the grains can reach several hundred nanometres.

Change in the grain structure of nanowires has been reported for a wide range of metals [38-41]. In this respect, the templated electrodeposition is similar to the metal deposition onto flat electrodes. In fact, if the single crystalline nuclei of a new phase are misoriented, their growth rate can be significantly different due to anisotropy of surface energy. Anisotropy in the growth rate results in the filtering of growth direction and columnar deposition. In the case of space limitation, the grain of suitable orientation can occupy the whole pore leading to the growth of single-crystalline nanowires if probability of secondary nucleation is low enough.

It is worth noting that in our case the nanowires remain polycrystalline even at a considerable distance from current collector. According to TEM images, certain grains exhibit cross-sectional dimensions of the same order as the pore diameters and form high-angle boundaries with neighbouring grains. This does not allow to exclude completely the secondary nucleation under the applied conditions of electrodeposition on the surface of single-crystalline grains, which is basically possible not only under purely kinetic, but also under mixed control.

Experimentally observed gradual evolution of the metal microstructure allows one to find the last piece of the puzzle concerning a long current decrease during templated electrodeposition: it can result from increase in metal grain size, leading to lower roughness of the nanowires edges and to corresponding decrease in real surface area of the electrode.

5. Conclusions

Scanning and transmission electron microscopy helped to discover the specific morphological and microstructural features of gold for various stages of templated electrodeposition from citric electrolyte containing $[Au(CN)_2]^-$ complex anion. First, it was evidenced that metal starts to grow in the form of nanotubes, which internal diameter is decreasing, and gradually progresses to the columnar

growth of nanowires. Clearly visible voids near the pore bottoms were observed. Second, the evolution of metal microstructure with the wire height was found, namely, larger size and more pronounced preferential orientation of crystals at the upper parts of the wire as compared to misoriented small crystals electrodeposited closer to the pore bottom. These observations correspond to deposition under mixed mode, with essential kinetic contribution, and in parallel with hydrogen evolution.

Coulometric estimates allowed to assign the pronounced maximum at current transients just to metal growth near the bottom, up to the height equal approximately to twice the pore diameter. In this specific region, the existence of the sputtered gold at the pore walls is unavoidable, as it penetrates to the pores in the course of current collector fabrication by physical vapour deposition. We considered possible effects of initial deposition on this sputtered gold.

The hypothesis of current increase with increase in the real surface area in the course of void formation was imposed to the system under study. Numerical simulations demonstrated that the void can be formed in case of very high diffusion contribution, and/or in presence of extensive continuous layer of sputtered gold. This results from faster growth of the upper parts of the nanotube due to the lower accessibility of $[Au(CN)_2]^-$ anions to the bottom of the pores.

However current behaviour under these conditions appears to be monotonic, in evident disagreement with experimental observations. This contradiction can be eliminated under assumption of discontinuous layer of sputtered gold grains, which surface is subsequently involved into electrodeposition of metal when the grains located near the bottom are growing and coalesce with small sputtered islands, initially isolated. The proposed assumption agrees qualitatively with the literature data on sputtered gold distribution inside the pores, and allows to explain the observed microstructure evolution. From “nanotechnological” point of view, the results are important to monitor nanowires growth. The appearance of the current maximum as a signature of voids formation, in combination with usual coulometric monitoring, is of special importance for controllable growth of short nanowires for, to say, optical/plasmonic applications [42, 43]. We should not hide the fact that our final hypothesis is inspired by general approach to current transient analysis widely accepted in electrocrystallization research [36], assuming coalescence/screening as the origin of current maxima, and the book and reviews of the late Professor Alexander Milchev played very important role in formulation of our hypotheses. A challenging problem for future is to provide quantitative description of these phenomena for the case of specific discontinuous distribution of support inside the nanopores.

Acknowledgments:

This work was supported by the Russian Science Foundation (Grant No. 18-73-10151). Anodic alumina templates were obtained under financial support of the RSF (Grant No. 19-73-10176). SEM images were recorded using scientific equipment purchased by the Lomonosov Moscow State University Program of Development. TEM analysis was performed using the equipment of the Shared Research Centre of the Federal Scientific Research Centre «Crystallography and Photonics» of the Russian Academy of Sciences supported by the Ministry of Science and Higher Education of the Russian Federation within the State assignment FSRC «Crystallography and Photonics» of RAS. GTs acknowledges the support of Pause program.

6. References

1. Sun L, Hao Y, Chien CL, Searson PC (2005) Tuning the properties of magnetic nanowires. IBM J Res Dev 49:79-102. https://doi.org/10.1147/rd.491.0079
2. Lai M, Riley DJ (2008) Templated electrosynthesis of nanomaterials and porous structures. J Colloid Interface Sci 323:203-212. https://doi.org/10.1016/j.jcis.2008.04.054
3. Napolskii KS, Roslyakov IV, Eliseev AA, Petukhov DI, Lukashin AV, Chen SF, Liu CP, Tsirlina GA (2011) Tuning the microstructure and functional properties of metal nanowire arrays via deposition potential. Electrochim Acta 56:2378-2384. https://doi.org/10.1016/j.electacta.2010.12.013
4. Masuda H, Fukuda K (1995) Ordered metal nanohole arrays made by a 2-step replication of honeycomb structures of anodic alumina. Science 268:1466-1468. https://doi.org/10.1126/science.268.5216.1466
5. Roslyakov IV, Shirin NA, Berekchiian MV, Shatalova TB, Garshev AV, Napolskii KS (2020) Coarse-grain alpha-alumina films with highly ordered porous structure. Micropor Mesopor Mat 294:109840. https://doi.org/10.1016/j.micromeso.2019.109840
6. Roslyakov IV, Shirin NA, Evdokimov PV, Berekchiian MV, Simonenko NP, Lyskov NV, Napolskii KS (2022) High-temperature annealing of porous anodic aluminium oxide prepared in selenic acid electrolyte. Surf Coat Tech 433:128080. https://doi.org/10.1016/j.surfcoat.2022.128080
7. Valizadeh S, George JM, Leisner P, Hultman L (2001) Electrochemical deposition of Co nanowire arrays; quantitative consideration of concentration profiles. Electrochim Acta 47:865-874. https://doi.org/10.1016/S0013-4686(01)00797-6
8. Motoyama M, Fukunaka Y, Sakka T, Ogata YH, Kikuchi S (2005) Electrochemical processing of Cu and Ni nanowire arrays. J Electroanal Chem 584:84-91. https://doi.org/10.1016/j.jelechem.2005.07.023
9. Blanco S, Vargas R, Mostany J, Borrás C, Scharifker B (2014) Modeling the Growth of Nanowire Arrays in Porous Membrane Templates. J Electrochem Soc 161:E3341-E3347. https://doi.org/10.1149/2.039408jes
10. Ghahremaninezhad A, Dolati A (2010) Diffusion-controlled growth model for electrodeposited cobalt nanowires in highly ordered aluminum oxide membrane. ECS Transactions 28:13-25. https://doi.org/10.1149/1.3503348
11. Davydov AD, Volgin VM (2016) Template electrodeposition of metals. Review. Russ J Electrochem 52:806-831. https://doi.org/10.1134/S1023193516090020

12. Bograchev DA, Davydov AD (2021) The role of common outer diffusion layer in the metal electrodeposition into template nanopores. Electrochim Acta 367:137405. https://doi.org/10.1016/j.electacta.2020.137405
13. Kalinin IA, Davydov AD, Leontiev AP, Napolskii KS, Sobolev A, Shatalov M, Zinigrad M, Bograchev D (2023) Influence of natural convection on the electrodeposition of copper nanowires in anodic aluminium oxide templates. Electrochim Acta 441:141766. https://doi.org/10.1016/j.electacta.2022.141766
14. Bograchev DA, Volgin VM, Davydov AD (2013) Simple model of mass transfer in template synthesis of metal ordered nanowire arrays. Electrochim Acta 96:1-7. https://doi.org/10.1016/j.electacta.2013.02.079
15. Noyan AA, Leontiev AP, Yakovlev MV, Roslyakov IV, Tsirlina GA, Napolskii KS (2017) Electrochemical growth of nanowires in anodic alumina templates: the role of pore branching. Electrochim Acta 226:60-68. https://doi.org/10.1016/j.electacta.2016.12.142
16. Srivastav AK, Shekhar R (2015) Nucleation and growth mechanism of Co–Pt alloy nanowires electrodeposited within alumina template. J Nanopart Res 17:14. https://doi.org/10.1007/s11051-014-2858-4
17. Shin S, Kong BH, Kim BS, Kim KM, Cho HK, Cho HH (2011) Over 95% of large-scale length uniformity in template-assisted electrodeposited nanowires by subzero-temperature electrodeposition. Nanoscale Res Lett 6:467. https://doi.org/10.1186/1556-276x-6-467
18. Scharifker B, Hills G (1983) Theoretical and experimental studies of multiple nucleation. Electrochim Acta 28:879-889. https://doi.org/10.1016/0013-4686(83)85163-9
19. Isaev VA, Grishenkova OV, Zaykov YP (2018) On the theory of 3D multiple nucleation with kinetic controlled growth. J Electroanal Chem 818:265-269. https://doi.org/10.1016/j.jelechem.2018.04.051
20. Cherevko S, Fu J, Kulyk N, Cho SM, Haam S, Chung CH (2009) Electrodeposition mechanism of palladium nanotube and nanowire arrays. J Nanosci Nanotechno 9:3154-3159. https://doi.org/10.1166/jnn.2009.011
21. Fu J, Cherevko S, Chung CH (2008) Electroplating of metal nanotubes and nanowires in a high aspect-ratio nanotemplate. Electrochem Commun 10:514-518. https://doi.org/10.1016/j.elecom.2008.01.015
22. Maas MG, Rodijk EJB, Wouter Maijenburg A, Blank DHA, ten Elshof JE (2011) Microstructure development in zinc oxide nanowires and iron oxohydroxide nanotubes by cathodic electrodeposition in nanopores. J Mater Res 26:2261-2267. https://doi.org/10.1557/jmr.2011.93
23. Motoyama M, Fukunaka Y, Sakka T, Ogata YH (2007) Initial stages of electrodeposition of metal nanowires in nanoporous templates. Electrochim Acta 53:205-212. https://doi.org/10.1016/j.electacta.2007.04.122
24. Lillo M, Losic D (2009) Pore opening detection for controlled dissolution of barrier oxide layer and fabrication of nanoporous alumina with through-hole morphology. J Membrane Sci 327:11-17. https://doi.org/10.1016/j.memsci.2008.11.033
25. Grigoras NK, Airaksinen VM, Franssila S, Coating of nanoporous membranes: Atomic layer deposition versus sputtering, Journal of Nanoscience and Nanotechnology, 2009, pp. 3763-3770.
26. Gojo M, Stanković VD, S.M. P (2008) Electrochemical deposition of gold in citrate solution containing thallium. Acta Chim Slov 55:330-337.
27. Sawaguchi T, Yamada T, Okinaka Y, Itaya K (1995) Electrochemical Scanning Tunneling Microscopy and Ultrahigh-Vacuum Investigation of Gold Cyanide Adlayers on Au(111) Formed in Aqueous Solution. J Phys Chem 99:14149-14155. https://doi.org/10.1021/j100038a056

28. Soleimany L, Dolati A, Ghorbani M (2010) A study on the kinetics of gold nanowire electrodeposition in polycarbonate templates. J Electroanal Chem 645:28-34. https://doi.org/10.1016/j.jelechem.2010.04.007
29. Seo B, Choi S, Kim J (2011) Simple Electrochemical Deposition of Au Nanoplates from Au(I) Cyanide Complexes and Their Electrocatalytic Activities. ACS Appl Mater Interfaces 3:441-446. https://doi.org/10.1021/am101018g
30. Levich VG (1962) Physicochemical Hydrodynamics. Prentice-Hall, New Jersey
31. Noyan AA, Kolesnik IV, Leont'ev AP, Napol'skii KS (2023) Electrocrystallization of Metals in Channels of Porous Films of Anodic Aluminum Oxide: The Real Template Structure and the Quantitative Model of Electrodeposition. Russ J Electrochem 59:489-500. https://doi.org/10.1134/S1023193523070078
32. Wheeler D, Josell D, Moffat TP (2003) Modeling Superconformal Electrodeposition Using The Level Set Method. J Electrochem Soc 150:C302. https://doi.org/10.1149/1.1562598
33. Adalsteinsson D, Sethian JA (1995) A Level Set Approach to a Unified Model for Etching, Deposition, and Lithography II: Three-Dimensional Simulations. J Comput Phys 122:348-366. https://doi.org/10.1006/jcph.1995.1221
34. Gough DA, Leypoldt JK (1979) Membrane-covered, rotated disk electrode. Anal Chem 51:439-444. https://doi.org/10.1021/ac50039a028
35. Miller CJ, Majda M (1986) Microporous Aluminum-Oxide Films at Electrodes .2. Studies of Electron-Transport in the Al2O3 Matrix Derivatized by Adsorption of Poly(4-Vinylpyridine). J Electroanal Chem 207:49-72. https://doi.org/10.1016/0022-0728(86)87062-0
36. Milchev A (2002) Electrocrystallization: Fundamentals of nucleation and growth. Springer, New York
37. Lee W, Scholz R, Nielsch K, Gösele U (2005) A Template-Based Electrochemical Method for the Synthesis of Multisegmented Metallic Nanotubes. Angew Chem Int Edit 44:6050-6054. https://doi.org/10.1002/anie.200501341
38. Huang XH, Li GH, Sun GZ, Dou XC, Li L, Zheng LX (2010) Initial Growth of Single-Crystalline Nanowires: From 3D Nucleation to 2D Growth. Nanoscale Res Lett 5:1057. https://doi.org/10.1007/s11671-010-9602-5
39. Shiave AI, Mohan R, Samykano M (2022) Crystal-structural characteristics of template-assisted electrodeposited cobalt nanowires: Effect of synthesis current density and temperature. MRS Advances 7:376-382. https://doi.org/10.1557/s43580-021-00137-7
40. Lyu S, Lei DY, Liu W, Yao H, Mo D, Chen Y, Hu P, Sun Y, Liu J, Duan JL (2015) Cyanide-free preparation of gold nanowires: Controlled crystallinity, crystallographic orientation and enhanced field emission. RSC Adv 5:32103-32109. https://doi.org/10.1039/c5ra00994d
41. Pan H, Sun H, Poh C, Feng Y, Lin J (2005) Single-crystal growth of metallic nanowires with preferred orientation. Nanotechnology 16:1559-1564. https://doi.org/10.1088/0957-4484/16/9/025
42. Kolmychek IA, Pomozov AR, Leontiev AP, Napolskii KS, Murzina TV (2018) Magneto-optical effects in hyperbolic metamaterials. Opt Lett 43:3917-3920. https://doi.org/10.1364/ol.43.003917
43. Kabashin AV, Evans P, Pastkovsky S, Hendren W, Wurtz GA, Atkinson R, Pollard R, Podolskiy VA, Zayats AV (2009) Plasmonic nanorod metamaterials for biosensing. Nat Mater 8:867-871. https://doi.org/10.1038/nmat2546